THE JOURNAL OF PHYSICAL CHEMISTRY A
A JOURNAL OF THE AMERICAN CHEMICAL SOCIETY

pubs.acs.org/JPCA

Perspective

Importance of Appropriately Regularizing the ML-MCTDH Equations of Motion

Haobin Wang* and Hans-Dieter Meyer*

Cite This: https://dx.doi.org/10.1021/acs.jpca.0c11221

Read Online

ACCESS | Metrics & More | Article Recommendations

ABSTRACT: The multiconfiguration time-dependent Hartree (MCTDH) method and its generalization, the multilayer MCTDH (ML-MCTDH), result in equations of motion (EOMs) that are singular when there are virtual orbitals—the unoccupied single-particle functions—in the wave function expansion. For decades this singularity had been numerically removed by regularizing the reduced density matrix. In this Perspective we discuss our recent proposal to regularize the coefficient tensor instead, which has significant impact on both the efficiency and correctness of the EOMs in MCTDH and ML-MCTDH for challenging problems. We further demonstrate that when the system becomes large such that it is necessary to use ML-MCTDH with many layers, it is much more important to employ this new regularization scheme. We illustrate this point by studying a spin−boson model with a large bath that contains up to 100 000 modes. We show that even in the weak coupling regime the new regularization scheme is required to quickly rotate the virtual orbitals into the correct directions in Hilbert space. We argue that this situation can be common for applying a time-dependent tensor network approach to any large enough system.

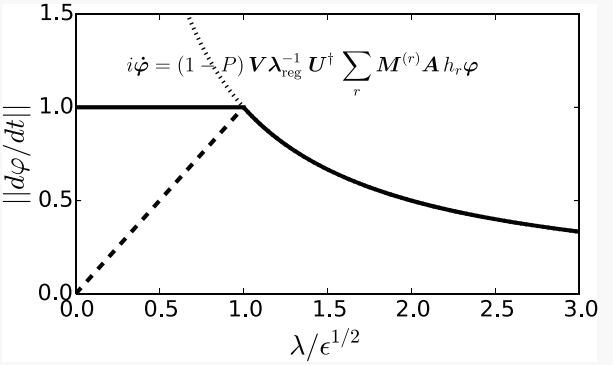

I. INTRODUCTION

The multiconfiguration time-dependent Hartree (MCTDH) method[1−5] was proposed 30 years ago[6] to treat larger molecular systems than those that could be handled by the standard, full configuration-interaction method. Since then, it enjoyed significant success in molecular quantum dynamics. It made its mark by being the first numerically exact approach to simulate the photoexcitation spectrum of pyrazine in full dimensionality.[7] It also afforded the study of model electron transfer reactions in condensed phases[8−11] that were once thought to be intractable by a basis set method. Other applications of MCTDH include simulating the IR spectrum for the Zundel cation ($H_5O_2^+$),[12−15] calculating the tunneling splitting in malonaldehyde,[16−19] and obtaining rate constants or cross sections for the H + CH_4 → H_2 + CH_3 reaction.[20−24]

The key ingredient of MCTDH is to replace the static orbitals in the standard method by the time-dependent orbitals, the so-called single particle functions (SPFs), and propagate both the expansion coefficients and the SPFs together. The SPFs still need to be represented, the simplest of which is to use static, primitive basis functions. This was used in the original MCTDH.[1−5] It all became natural to think about adopting the same MCTDH philosophy on the SPFs themselves, and even doing so recursively. The multilayer MCTDH (ML-MCTDH)[25−28] was proposed to achieve this. In ML-MCTDH the wave function is expressed by a recursive layered expansion, with only the bottom layer represented by static basis functions. The Dirac−Frenkel variational principle[29] is then applied to this wave function ansatz, which results in a set of coupled ordinary differential equations that define the time evolution for ML-MCTDH.[25−28]

ML-MCTDH has been designed to treat much larger systems. Despite its name ("Hartree"), it is applicable to identical particles by using a second quantized re-formulation.[30] Furthermore, it is not limited to only simulating real time quantum dynamics but can also be applied to computing eigenstates[31,32] or equilibrium reduced density matrices[33] for systems with many degrees of freedom. Its application in quantum dynamics includes the study of charge transfer reactions,[34−46] quantum transport,[47−54] surface scattering,[55] photodissociation of a molecule embedded in a complex,[56] vibronic dynamics,[57] reactive scattering,[23,24] exciton vibrational dynamics,[58−60] and singlet fission.[61,62]

There has also been significant interest in other fields, e.g., applied mathematics, in the form of the ML-MCTDH tensor contraction. The original MCTDH approach utilizes the so-

Received: December 16, 2020
Revised: February 14, 2021

called Tucker form[63] of tensor decomposition. The ML-MCTDH expansion of a wave function was later therefore called the hierarchical Tucker (H-Tucker) form by mathematicians.[64−66] It is also called a tree tensor network. Though ML-MCTDH (or the H-Tucker format) has a rather general form, practical implementations often refer to a binary branching or a similarly balanced tree structure.[65] A notable exception to this is a special skewed tree structure that has gained popularity recently, which is called the tensor train format in mathematics and the matrix-product states in physics.[67]

MCTDH and ML-MCTDH approximate the exact wave function by tensor contraction. The accuracy of such a contraction increases when the number of SPFs, hence the configuration space, increases for all nodes. (As discussed below, a *node* is a point in the ML-tree where a SPF of an upper layer is expanded into the SPFs of a lower layer. A node is labeled by the index z and is represented mathematically by a coefficient tensor $A^{z}_{m;J}$. And a *mode*, q_κ, denotes a collection of several degrees of freedom.) An important indicator for convergence are the eigenvalues $p_i^{(z,\kappa)}$ of the reduced density matrix $\rho^{(z,\kappa)}$ for each node z and mode κ, the so-called natural populations. If the smallest $p_i^{(z,\kappa)}$ approaches (or in fact is) zero, the correlation effect has been completely accounted for in this node. This is usually a good thing, but it creates a numerical problem in the equations of motion for the SPFs in this mode: they become singular. The situation is ubiquitous at short times when most of the SPFs are unoccupied. Because of this numerical singularity, there are some concerns in the mathematics community in spite of the apparent success of MCTDH and ML-MCTDH.

It should be noted that in practice a regularization procedure was applied to numerically remove the singularities, in essence setting the zero eigenvalues $p_i^{(z,\kappa)}$ of the reduced density matrix $\rho^{(z,\kappa)}$ to some regularization parameter ϵ. The thus regularized density matrix can be safely inverted, and convergence can be checked with decreasing ϵ. This regularization procedure has been used for decades by almost all researchers in this field. In most situations it worked just fine. However, we have shown recently[68,69] that for challenging cases much better results were obtained when the matrix unfolding of the expansion coefficients are regularized. The new regularization scheme rotates the unoccupied SPFs toward their optimal directions much more quickly than the previous density matrix-based regularization and may thus increase both the accuracy and efficiency of the time propagation. In contrast to the "singularity-free" type integrator,[70,71] our regularization scheme takes the advantage of the singularity to effectively exploit the optimal Hilbert subspace so that correct results can be obtained.

In this Perspective we discuss our new regularization scheme[68,69] with a focus on ML-MCTDH simulations for large systems. The necessity of using many layers to handle such systems makes the new approach much more important. We will show that, for very large systems, the previous density matrix-based regularization scheme fails even for weak coupling physical regimes, whereas the new scheme with a reasonably small regularization parameter ϵ is the only viable option. This has significant implications for further developments of time-dependent tensor network methods for large systems.

The paper is organized as follows. In section II we discuss how to apply our new regularization scheme to the MCTDH equations of motion. We do so first because the MCTDH equations are much simpler than those in ML-MCTDH, and the most important aspect of the new regularization scheme is almost the same between MCTDH and ML-MCTDH. Then in section III we extend the scheme to ML-MCTDH. In section IV we demonstrate the importance of our approach by considering several examples of the spin−boson model, and pushing the model limit to 100 000 bath modes. Section V discusses our findings.

II. REGULARIZING THE MCTDH EQUATIONS OF MOTION

II.A. The MCTDH Equations of Motion. The MCTDH wave function is written as[1−5]

$$\begin{aligned}\Psi(Q_1, ..., Q_f, t) &= \Psi(q_1, ..., q_p, t)\\ &= \sum_{j_1=1}^{n_1} \cdots \sum_{j_p=1}^{n_p} A_{j_1 \cdots j_p}(t) \prod_{\kappa=1}^{p} \varphi_{j_\kappa}^{(\kappa)}(q_\kappa, t)\\ &= \sum_J A_J \Phi_J\end{aligned} \tag{2.1}$$

where f denotes the number of physical coordinates, Q_i, and where p denotes the number of *modes*, q_κ (also called *particles* or *logical coordinates*[26]) and $\kappa = 1, ..., p$ labels the modes. Each mode, $q_\kappa = (Q_a, Q_b, ...)$, defines a physical subspace that may contain one to several physical degrees of freedom, typically, 1, 2, or 3, sometimes more. The orbital functions φ are called *single particle functions* (SPF) and there are n_κ SPFs for the κth node. The symbol $J = (j_1, ..., j_p)$ is a composite index and the configuration is defined as the Hartree product $|\Phi_J\rangle \equiv \prod_{\kappa=1}^{p} |\varphi_{j_\kappa}^{(\kappa)}\rangle$. In MCTDH the SPFs are expanded with static primitive basis functions χ multiplied by time-dependent coefficients

$$\varphi_{j_\kappa}^{(\kappa)}(q_\kappa, t) = \sum_{l=1}^{N_\kappa} c_{j_\kappa,l}^{(\kappa)}(t)\, \chi_l^{(\kappa)}(q_\kappa) \tag{2.2}$$

where $N_\kappa \geq n_\kappa$ denotes the number of primitive functions of the κth node.

The Dirac−Frenkel variational principle[29] is then applied to the MCTDH wave function above for all time-dependent variables. Adopting the standard gauge condition, $i\langle\varphi_l^{(\kappa)}|\dot{\varphi}_j^{(\kappa)}\rangle = 0$, the equations of motion are (the overhead dot denotes time derivative)

$$i\dot{A}_J = \sum_L \langle\Phi_J|H|\Phi_L\rangle A_L \tag{2.3}$$

$$i\boldsymbol{\rho}^{(\kappa)}\dot{\boldsymbol{\varphi}}^{(\kappa)} = (1 - P^{(\kappa)})\langle\mathbf{H}\rangle^{(\kappa)}\boldsymbol{\varphi}^{(\kappa)} \tag{2.4}$$

where $\boldsymbol{\rho}^{(\kappa)}$ is the reduced density matrix, $\langle\mathbf{H}\rangle^{(\kappa)}$ is the mean-field operator, $\boldsymbol{\varphi}^{(\kappa)}$ is a vector of SPFs, i.e., $\boldsymbol{\varphi}^{(\kappa)} = (\varphi_1^{(\kappa)}), ..., \varphi_{n_\kappa}^{(\kappa)\mathrm{T}}$, $\dot{\boldsymbol{\varphi}}^{(\kappa)}$ is the vector of the corresponding time derivative of SPFs, and $P^{(\kappa)}$ is the projector

$$P^{(\kappa)} = \sum_{j=1}^{n_\kappa} |\varphi_j^{(\kappa)}\rangle\langle\varphi_j^{(\kappa)}| \tag{2.5}$$

To define the reduced density matrix $\boldsymbol{\rho}^{(\kappa)}$ and the mean-field operator $\langle\mathbf{H}\rangle^{(\kappa)}$, one introduces single-hole functions that project out particular SPFs

$$\Psi_l^{(\kappa)} = \sum_{J^\kappa} A_{J^\kappa,l}\Phi_{J^\kappa} \tag{2.6}$$

with

https://dx.doi.org/10.1021/acs.jpca.0c11221
J. Phys. Chem. A XXXX, XXX, XXX−XXX

$$J^{\kappa} = (j_1, ..., j_{\kappa-1}, j_{\kappa+1}, ..., j_p)$$

$$\Phi_{J^{\kappa}} = \prod_{\nu=1,\nu\neq\kappa}^{p} \varphi_{j_\nu}^{(\nu)}$$

$$A_{J^{\kappa},l} = A_{j_1,...,j_{\kappa-1},l,j_{\kappa+1},...,j_p} \tag{2.7}$$

The matrix elements for $\boldsymbol{\rho}^{(\kappa)}$ and $\langle \mathbf{H} \rangle^{(\kappa)}$ are now defined as

$$\rho_{jl}^{(\kappa)} = \langle \Psi_j^{(\kappa)} | \Psi_l^{(\kappa)} \rangle = \sum_{J^{\kappa}} A^*_{J^{\kappa},j} A_{J^{\kappa},l} \tag{2.8}$$

and

$$\langle H \rangle_{jl}^{(\kappa)} = \langle \Psi_j^{(\kappa)} | H | \Psi_l^{(\kappa)} \rangle \tag{2.9}$$

In MCTDH the Hamiltonian is usually written in a sum-of-products form

$$H = \sum_{r=1}^{s} c_r \prod_{\kappa=1}^{p} h_r^{(\kappa)} \tag{2.10}$$

where c_r is a number and $h_r^{(\kappa)}$ operates on the κth node only. Using the sum-of-products form, the mean-field operators can be written as

$$\langle H \rangle_{jl}^{(\kappa)} = \sum_{r=1}^{s} \mathcal{H}_{jl}^{(\kappa,r)} h_r^{(\kappa)} \tag{2.11}$$

where the mean-field matrix $\mathcal{H}^{(\kappa,r)}$ has elements

$$\mathcal{H}_{jl}^{(\kappa,r)} = \sum_{J^{\kappa}} \sum_{L^{\kappa}} A^*_{J^{\kappa},j} M^{(\kappa,r)}_{J^{\kappa},L^{\kappa}} A_{L^{\kappa},l} \tag{2.12}$$

in which

$$M_{J^{\kappa},L^{\kappa}}^{(\kappa,r)} = c_r \prod_{\nu=1,\nu\neq\kappa}^{p} m_{j_\nu,l_\nu}^{(\nu,r)} \tag{2.13}$$

with

$$m_{j,l}^{(\kappa,r)} = \langle \varphi_j^{(\kappa)} | h_r^{(\kappa)} | \varphi_l^{(\kappa)} \rangle \tag{2.14}$$

II.B. Regularization of the MCTDH Equations of Motion. The time derivatives for the expansion coefficients in eq 2.3 are explicit and can be obtained straightforwardly. However, the time derivatives for the SPFs in eq 2.4 require solving a system of linear equations for the unknown $\dot{\boldsymbol{\varphi}}^{(\kappa)}$. There are two questions regarding eq 2.4: First, is the linear system consistent? I.e., does the system possess at least one solution? Second, if solutions exist, is the solution unique? Unfortunately, when the reduced density matrix $\boldsymbol{\rho}^{(\kappa)}$ is singular, there is no guarantee of either of them.

In MCTDH only the occupied SPFs are well-defined initially. The unoccupied SPFs can be chosen at complete random. There is no problem with it because these unoccupied SPFs make no contribution to the wave function. This redundancy makes it possible, at least in principle, to choose the initial unoccupied SPFs to make the linear system consistent, thus answering the first question. One can also go beyond the first order equations to define the optimal form of the initially unoccupied SPFs, as discussed by Manthe,[72] and also by Lee and Fischer,[73] and by Mendive-Tapia and Meyer.[74]

The answer is almost always no to the second question if $\boldsymbol{\rho}^{(\kappa)}$ is singular. That is, even if the system is consistent, it is *underdetermined*, which means there are fewer equations than unknowns. This is also a manifestation of the zero contribution from the unoccupied SPFs, which provides infinite possibilities for these SPFs. In practice, one may write a formal solution to eq 2.4 as

$$\mathrm{i}\dot{\boldsymbol{\varphi}}^{(\kappa)} = (1 - P^{(\kappa)})(\boldsymbol{\rho}_{\mathrm{reg}}^{(\kappa)})^{-1} \langle \mathbf{H} \rangle^{(\kappa)} \boldsymbol{\varphi}^{(\kappa)} \tag{2.15}$$

where $(\boldsymbol{\rho}_{\mathrm{reg}}^{(\kappa)})^{-1}$ is a *pseudoinverse* of the reduced density matrix $\boldsymbol{\rho}^{(\kappa)}$, e.g., first regularizing $\boldsymbol{\rho}^{(\kappa)}$ by replacing its zero eigenvalues by some regularization parameter ϵ and then inverting the resulting regular matrix. For a particular ϵ the solution is uniquely defined above, and this was the standard regularization approach used previously. It is hoped that the solution dependence on ϵ is weak such that convergence can be achieved by decreasing ϵ. In most situations exploited so far this was indeed the case. The MCTDH equations of motion show a "self-healing" effect. Unsuitable SPFs are rotated quickly into their "correct direction" in Hilbert space, i.e., into the direction in which they contribute optimally to the expansion of the wave function.

The rotation of the unoccupied SPFs nevertheless takes some time. If this time is comparable to or longer than the physical time scale, then the MCTDH wave function is no longer an accurate approximation to the true wave function. Our recently proposed new regularization scheme aims at solving this problem. One can, of course, define the initially unoccupied SPFs to let them point into the optimal direction, as done by Manthe[72] and others.[73,74] Our approach is much simpler to implement and works well for very challenging cases.

The starting point is to introduce the matrix unfolding of the coefficient tensor for the κth node A_{J^{κ},j_κ} as an element of the matrix $\mathbf{A}^{(\kappa)}$ of dimension $(\bar{n}_\kappa \times n_\kappa)$, with $\bar{n}_\kappa = \prod_{\nu=1,\nu\neq\kappa}^{p} n_\nu$. Then some of the equations above are written as matrix products

$$\boldsymbol{\rho}^{(\kappa)} = \mathbf{A}^{(\kappa)\dagger} \mathbf{A}^{(\kappa)} \tag{2.16}$$

$$\mathcal{H}^{(\kappa,r)} = \mathbf{A}^{(\kappa)\dagger} \mathbf{M}^{(\kappa,r)} \mathbf{A}^{(\kappa)} \tag{2.17}$$

and eq 2.4 is written as

$$\mathrm{i}(\mathbf{A}^{(\kappa)\dagger}\mathbf{A}^{(\kappa)})\dot{\boldsymbol{\varphi}}^{(\kappa)} = (1 - P^{(\kappa)})\mathbf{A}^{(\kappa)\dagger} \sum_r \mathbf{M}^{(\kappa,r)} \mathbf{A}^{(\kappa)} h_r^{(\kappa)} \boldsymbol{\varphi}^{(\kappa)} \tag{2.18}$$

Now we can write matrix $\mathbf{A}^{(\kappa)}$ as a singular value decomposition (SVD), and for simplicity we drop the mode index κ in the following expressions

$$\mathbf{A} = \mathbf{U}\boldsymbol{\lambda}\mathbf{V}^{\dagger} \tag{2.19}$$

Instead of regularizing the reduced density, our new approach regularizes $\mathbf{A}$

$$\mathbf{A}_{\mathrm{reg}} = \mathbf{U}\boldsymbol{\lambda}_{\mathrm{reg}}\mathbf{V}^{\dagger} \tag{2.20}$$

which can be done, for example, via a simple procedure

$$\lambda_j^{\mathrm{reg}} = \max(\lambda_j, \epsilon^{1/2}) \tag{2.21}$$

Inserting (2.20) into (2.18) and making use of the unitarity of $\mathbf{U}$ and $\mathbf{V}$, the new regularization scheme yields

$$\mathrm{i}\dot{\boldsymbol{\varphi}} = (1 - P)\mathbf{V}\boldsymbol{\lambda}_{\mathrm{reg}}{}^{-1}\mathbf{U}^{\dagger} \sum_r \mathbf{M}^{(r)} \mathbf{A} h_r \boldsymbol{\varphi} \tag{2.22}$$

where the last coefficient matrix is not regularized in order to be minimally invasive.

https://dx.doi.org/10.1021/acs.jpca.0c11221
J. Phys. Chem. A XXXX, XXX, XXX−XXX

The connection between the old and the current regularization approach is given via the reduced density matrix

$$\boldsymbol{\rho} = \mathbf{A}^{\dagger}\mathbf{A} = \mathbf{V}\boldsymbol{\lambda}^{2}\mathbf{V}^{\dagger} \tag{2.23}$$

which recognizes $p_j = \lambda_j^2$ as the natural populations. By transforming a set of SPFs with $\mathbf{V}^{\dagger}$, one obtains the so-called natural orbitals. The old approach (2.15) only regularizes the reduced density matrix. Put it in context with (2.22), it reads

$$i\dot{\boldsymbol{\varphi}} = (1 - P)\mathbf{V}\boldsymbol{\lambda}_{\mathrm{reg}}{}^{-2}\boldsymbol{\lambda}\mathbf{U}^{\dagger}\sum_{r}\mathbf{M}^{(r)}\mathbf{A}h_r\boldsymbol{\varphi} \tag{2.24}$$

This small difference has a profound impact on the performance.[68,69]

To visualize the difference between eqs 2.22 and 2.24, we plot in Figure 1 the modulus of the time derivative of a natural orbital

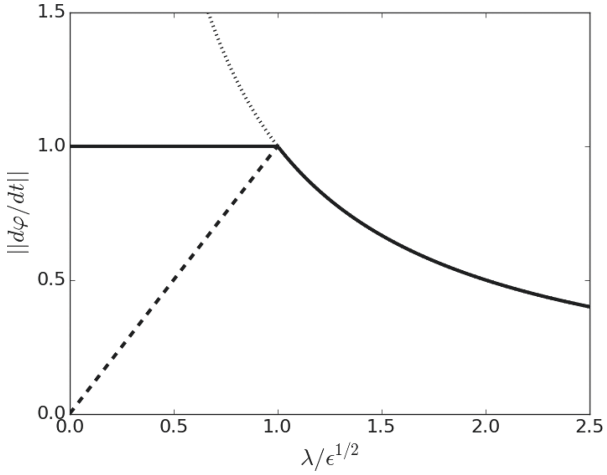

Figure 1. Comparison of the two regularization schemes. The full line shows symbolically the speed of orbital rotation (in arbitrary units) of the new regularization scheme versus the singular value λ, i.e., the function $\lambda_{\mathrm{reg}}{}^{-1}$. The dotted line is the continuation of the $1/\lambda$ curve for small λ. The dashed line displays the speed of orbital rotation of the old regularization scheme, i.e., $\lambda_{\mathrm{reg}}{}^{-2}\lambda$, which is λ/ϵ for $\lambda \leq \epsilon^{1/2}$ and $1/\lambda$ otherwise.

versus λ. For natural orbitals the transformation matrix $\mathbf{V}$ becomes a unit matrix and the time derivative is proportional to $\lambda_{\mathrm{reg}}{}^{-1}$ or $\lambda_{\mathrm{reg}}{}^{-2}\lambda$, respectively. The new regularization (full line) limits the time derivative to a constant value. Note in particular that the time derivative, i.e., the speed of rotation of the natural orbital, is large when λ vanishes. For the old regularization scheme, on the other hand, the time derivative vanishes when λ approaches zero (dashed line). Figure 1 makes it clear that the new scheme rotates unoccupied or weakly occupied natural orbitals much faster than the old scheme. Moreover, truly unoccupied natural orbitals, $\lambda = 0$, are not at all rotated by the old scheme! The unoccupied SPF has first to gain some tiny occupation (of the order of ϵ) by **A**-vector propagation to be able to get rotated. As the unoccupied SPFs are in general not orthogonal to the optimal ones, they acquire some tiny occupation during the first steps of propagation and the old regularization scheme works fine. But if the SPFs are of rather high dimensionality, a situation that frequently appears in the upper layers of an ML-MCTDH calculation, then it is more likely that the initially unoccupied SPFs are (almost) orthogonal to the optimal ones. This makes it clear that the new regularization scheme is more important for ML-MCTDH than for MCTDH.

An interesting situation appears in case of symmetries. Consider rotational excitation of H_2 by collision. Starting from the rotational ground state, $j = 0$, only even j-states can be populated due to symmetry. If one (erroneously) provides a $j = 1$ Legendre function as unoccupied SPF, this SPF cannot acquire occupation by **A**-vector propagation due to the symmetry restriction and thus cannot be rotated by the old scheme. It will stay in the $j = 1$ state for all times and will be useless for improving the expansion of the wave function. However, when the new regularization scheme is used, the algorithm will immediately start to rotate the $j = 1$ SPF to an even j-state.

III. EXTENDING THE REGULARIZATION SCHEME TO ML-MCTDH

The principle idea remains the same when extending the new regularization scheme to ML-MCTDH. However, the ML-MCTDH equations of motion[25−28] are much more complicated than the MCTDH ones, and it is not at all obvious how to implement the new scheme. In particular, a recursive formulation is needed to treat an arbitrary number of layers. Here we outline a few salient features how this could be done. For more details the readers may consult ref 69.

III.A. The ML-MCTDH Equations of Motion. To describe an ML-MCTDH wave function a more complex nomenclature is needed. We rewrite eq 2.1 in ML-MCTDH nomenclature as

$$\Psi(q_1^1, \ldots, q_{p^1}^1, t) = \sum_{j_1}^{n_1^1}\cdots\sum_{j_{p^1}}^{n_{p^1}^1} A^1_{1;j_1,\ldots,j_{p^1}}(t)\cdot\varphi_{j_1}^{(1;1)}(q_1^1, t)\cdot\ldots\cdot\varphi_{j_p^1}^{(1;p^1)}(q_{p^1}^1, t) \tag{3.1}$$

The upper index 1 indicates that the quantities are for the layer number 1, also called top layer. In the MCTDH method, which is equivalent to a two-layer[75] ML-MCTDH approach, the multidimensional SPFs are given by the second-layer equation (cf. eq 2.22)

$$\varphi_m^{1;\kappa_1}(q_{\kappa_1}^1, t) = \sum_{j_1}^{N_1^{\kappa_1}}\cdots\sum_{j_{p^{2;\kappa_1}}}^{N_{p^{2;\kappa_1}}^{\kappa_1}} A^{2;\kappa_1}_{m;j_1,\ldots,j_{p^{2;\kappa_1}}}(t)\cdot\chi_{j_1}^{(\kappa_1,1)}(q_1^{2;\kappa_1})\cdot\ldots\cdot\chi_{j_{p^{2;\kappa_1}}}^{(\kappa_1,p^{2;\kappa_1})}(q_{p^{2;\kappa_1}}^{2;\kappa_1}) \tag{3.2}$$

where χ denotes a primitive basis function and $q_{\kappa_2}^{2;\kappa_1}$ is here the physical coordinate (or a combined mode) of the κ_2th DOF of the node $(2;\kappa_1)$, which has $p^{2;\kappa_1}$ branches.

Adding additional layers, one has to specify which node of the ML-tree is under consideration. For this it is convenient to introduce the symbol

$$z = l;\ \kappa_1, \ldots, \kappa_{l-1} \quad \text{and} \quad z - 1 = l - 1;\ \kappa_1, \ldots, \kappa_{l-2} \tag{3.3}$$

Here l denotes the layer and $\kappa_1, \ldots, \kappa_{l-1}$ denote the modes of the layers above which leads to the node under consideration. Hence, z precisely defines one particular node in the ML-tree.[26,27]

The ML expansion can now be written in full generality

https://dx.doi.org/10.1021/acs.jpca.0c11221
J. Phys. Chem. A XXXX, XXX, XXX−XXX

$$\varphi_m^{z-1,\kappa_{l-1}}(q_{\kappa_{l-1}}^{z-1}) = \sum_{j_1}^{n_1^z} \cdots \sum_{j_{p^z}}^{n_{p_z}^z} A_{m;j_1,\cdots,j_{p^z}}^{z} \prod_{\kappa_l=1}^{p^z} \varphi_{j_{\kappa_l}}^{z,\kappa_l}(q_{\kappa_l}^{z}) = \sum_J A_{m;J}^{z} \cdot \Phi_J^z(q_{\kappa_{l-1}}^{z-1}) \tag{3.4}$$

which implicitly defines the configurations Φ_J^z and the composite index J, and where the coordinates are combined as

$$q_{\kappa_{l-1}}^{z-1} = \{q_1^z, \ldots, q_{p^z}^z\} \tag{3.5}$$

eq 3.4 holds also for the top layer if one defines q^0 as the combination of all DOFs and sets $\Psi(q^0, t) = \varphi_1^0(q^0, t)$, and it also holds for the bottom layer if one identifies φ^{z,κ_l} with the primitive function χ^{κ_l}, when z points to a bottom node. Hence eq 3.4 holds for all layers.

The ML-MCTDH equations of motion for the SPFs are formally the same for all layers, which has the same form as eq 2.4

$$\mathrm{i}\sum_n (\rho^{z,\kappa_l})_{mn} \cdot \frac{\partial \varphi_n^{z,\kappa_l}}{\partial t} = (1 - \hat{P}^{z,\kappa_l}) \sum_n \langle \hat{H} \rangle_{mn}^{z,\kappa_l} \varphi_n^{z,\kappa_l} \tag{3.6}$$

where $\hat{P}^{z,\kappa_l} = \sum_n |\varphi_n^{z,\kappa_l}\rangle\langle\varphi_n^{z,\kappa_l}|$ is the projector onto the space spanned by the φ_n^{z,κ_l} SPFs, ρ^{z,κ_l} is a density matrix, and $\langle \hat{H} \rangle^{z,\kappa_l}$ is a matrix of mean-field operators acting on the φ_n^{z,κ_l} functions. The difference between ML-MCTDH and MCTDH lies on how the reduced density matrix is constructed

$$\rho_{ij}^{z,\kappa_l} = \sum_{a,b=1}^{n_{\kappa_{l-1}}^{z-1}} \rho_{ab}^{z-1,\kappa_{l-1}} \sum_{J^{\kappa_l}} A_{a;J^{\kappa_l},i}^{z*} A_{b;J^{\kappa_l},j}^{z} \tag{3.7}$$

That is, the reduced density matrix ρ^{z,κ_l} for a node z and mode κ_l requires the expansion coefficients of the present node z and reduced density matrix $\rho^{z-1,\kappa_{l-1}}$ of the parent node. This recursion means ρ^{z,κ_l} formally involves the expansion coefficients of both zth and $(z-1)$th nodes, except for the top layer, where eq 2.8 is still valid. A similar expression applies to the mean-field operator matrix.[25−28]

III.B. Regularization of the ML-MCTDH Equations of Motion. If one tries to express ρ^{z,κ_l} using a similar matrix unfolding as for the MCTDH case described in the previous section, e.g., eq 2.16, then one has to deal with the full-length products of the expansion coefficients of two adjacent layers. The resulting matrix size can be huge. Instead, we insert the diagonal form of the density,

$$\boldsymbol{\rho}^{z-1,\kappa_l} = \mathbf{V}^{z-1,\kappa_l} (\boldsymbol{\lambda}^{z-1,\kappa_l})^2 \mathbf{V}^{z,\kappa_l \dagger} \tag{3.8}$$

into the recursion formula for the density, eq 3.7

$$\begin{aligned} \rho_{ij}^{z,\kappa_l} &= \sum_{J^{K}l} \sum_{a,b,c=1}^{n_{\kappa_{l-1}}^{z-1}} A_{a;J^{K}l,i}^{z*} V_{ac}^{z-1,\kappa_{l-1}} (\lambda_c^{z-1,\kappa_{l-1}})^2 \\ &\quad \times V_{bc}^{z-1,\kappa_{l-1}*} A_{b;J^{\kappa_l},j}^{z} \\ &= \sum_{J^{\kappa_l}} \sum_a \tilde{A}_{a;J^{\kappa_l},i}^{z,\kappa_l *} A_{a;J^{\kappa_l},j}^{z,\kappa_l} \\ &= \sum_{m=1}^{n_{\kappa_l}^z} V_{im}^{z,\kappa_l} (\lambda_m^{z,\kappa_l})^2 V_{jm}^{z,\kappa_l *} \end{aligned} \tag{3.9}$$

where in the first step we have introduced the definition

$$\tilde{A}_{a;J^{\kappa_l},j}^{z,\kappa_l} = \sum_{c=1}^{n_{\kappa_{l-1}}^{z-1}} \lambda_a^{z-1,\kappa_{l-1}} V_{ca}^{z-1,\kappa_{l-1}*} A_{c;J^{\kappa_l},j}^{z} \tag{3.10}$$

and in the second step we have made use of a singular value decomposition of $\tilde{A}$, where $(a; J^{\kappa_l})$ is considered a composite index.

$$\tilde{A}_{a;J^{\kappa_l},j}^{z,\kappa_l} = \sum_{k=1}^{n_{\kappa_l}^z} U_{a;J^{\kappa_l},k}^{z,\kappa_l} \lambda_k^{z,\kappa_l} V_{jk}^{z,\kappa_l *} \tag{3.11}$$

This is a practical implementation as the matrix unfolding $\tilde{A}^{z,\kappa_l}$ is usually not quite large. Equation 3.9 shows how to recursively perform the SVD and diagonalize the reduced density matrix, where the first layer [the base case (3.8)] is given by eqs 2.16 and 2.23. The recursion for the matrix U in the SVD can be done in a similar fashion, which is a minor (but tedious) detail that can be found in ref 69.

Once the SVD can be defined recursively as in eqs 3.9−3.11, regularization can be done similarly as for the MCTDH case described in the previous section. As for the old integration scheme, ML-MCTDH requires two sweeps to complete the equations of motion. First, the h-matrix elements are build bottom up, until the top-level mean-field matrices are build. Then top-down recursions for the mean fields are performed, which requires the building of $\tilde{A}$ and its SVD. The regularized equations of motion that correspond to (3.6) are thus generated.

IV. ILLUSTRATED EXAMPLES

In our previous work[68,69] we have tested the new regularization scheme on the spin−boson model.[76,77] Here we do it again but for much bigger systems. The spin−boson Hamiltonian has been widely used to model electron transfer reactions. It contains two electronic states ($|\phi_1\rangle$ and $|\phi_2\rangle$) linearly coupled to a bath of harmonic oscillators. Using mass-weighted coordinates the Hamiltonian reads

$$H = D\sigma_z + \Delta\sigma_x + \frac{1}{2}\sum_{j=1}^{N} (p_j^2 + \omega_j^2 q_j^2) + \sigma_z \sum_{j=1}^{N} c_j q_j \tag{4.1}$$

where σ_x and σ_z are Pauli matrices

$$\sigma_x = |\phi_1\rangle\langle\phi_2| + |\phi_2\rangle\langle\phi_1| \tag{4.2a}$$

$$\sigma_z = |\phi_1\rangle\langle\phi_1| - |\phi_2\rangle\langle\phi_2| \tag{4.2b}$$

The properties of the bath that influence the dynamics of the two-state subsystem are specified by the spectral density function[76,77]

$$J(\omega) = \frac{\pi}{2}\sum_j \frac{c_j^2}{\omega_j} \delta(\omega - \omega_j) \tag{4.3}$$

In the test examples below we use an Ohmic (linear) spectral density with an exponential cutoff

$$J(\omega) = \frac{\pi}{2} \alpha\omega \mathrm{e}^{-\omega/\omega_c} \tag{4.4}$$

where α is the dimensionless Kondo parameter that characterizes the system−bath coupling strength and ω_c is the cutoff frequency of the bath. The continuous bath spectral density of eq 4.4 can be discretized to the form of eq 4.3 via the relation[9,25]

https://dx.doi.org/10.1021/acs.jpca.0c11221
J. Phys. Chem. A XXXX, XXX, XXX−XXX

$$c_j^2 = \frac{2}{\pi}\omega_j \frac{J(\omega_j)}{\rho(\omega_j)} \tag{4.5}$$

in which the density of frequency $\rho(\omega)$ is defined from the integral relation

$$\int_0^{\omega_j} d\omega\ \rho(\omega) = j \qquad j = 1, ..., N \tag{4.6a}$$

In this work, $\rho(\omega)$ is chosen as

$$\rho(\omega) = \frac{N+1}{\omega_c} e^{-\omega/\omega_c} \tag{4.6b}$$

where $\omega_{N+1} = \infty$ is removed from the simulation.

IV.A. An Example of Strong Coupling. First we consider an example of strong system−bath coupling, with Kondo parameter $\alpha = 2$, and other parameters $D/\Delta = 0$, $\omega/\Delta = 25$. The dynamical property examined here is the time-dependent population (difference) of the two-level subsystem

$$P(t) \equiv \langle \sigma_z(t) \rangle = \langle \Psi(t) | \sigma_z | \Psi(t) \rangle \tag{4.7}$$

where initially the system state $|\phi_1\rangle$ is populated and the bath starts from its ground state for all the modes.

The first case is for a bath of 10 000 modes, with its $P(t)$ displayed in Figure 2. Here we use dimensionless units, but for a typical characteristic frequency $\omega_c = 52.1$ cm^{-1}, the wave function is propagated to 2000 fs. A 7-layer ML-MCTDH was used in the simulation. The first layer has five bath nodes and one node for the two system states. There are eight SPFs per bath node, resulting in a total of $8^5 \times 2 = 65\,536$ configurations for the first layer. For the other layers, there are up to three child nodes under each parent node, with five SPFs per node. Mode combination and adiabatic basis contraction are used for each bottom layer node, which holds up to 4 bath modes. A variable stepsize predictor-corrector ordinary differential equation (ODE) solver was used in the time integration, with its absolute tolerance set to 10^{-10} and relative tolerance set to 10^{-6}. These parameters have passed extensive convergence tests.

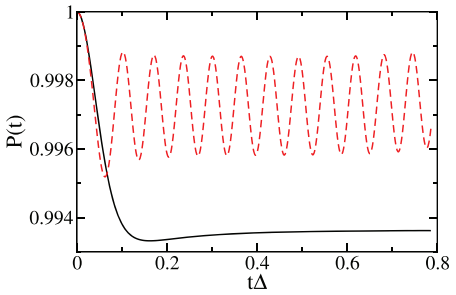

Figure 2. Time dependence of $P(t) = \langle \sigma_z(t) \rangle$ for $D/\Delta = 0$, $\alpha = 2$, and $\omega_c/\Delta = 25$. A bath of 10 000 modes is used in a seven-layer ML-MCTDH simulation. The solid line is the reference $P(t)$ employing the new regularization scheme with $\epsilon = 10^{-32}$, where the dashed line is (the incorrect) $P(t)$ obtained using the old regularization scheme with $\epsilon = 10^{-8}$.

For the same regularization parameter ϵ the new regularization scheme has an added bonus. Compared with regularization of the reduced density matrix, eq 2.23, which requires replacing small λ_j^2 with ϵ, the new regularization scheme (2.20) replaces λ_j with $\epsilon^{1/2}$ as shown in (2.21). This allows a smaller ϵ to be used in the new scheme for more difficult cases. If 10^{-16} is approximately the double precision limit, then this is the smallest ϵ that can be used in the old scheme. The new scheme, however, can be extended to $\epsilon = 10^{-32}$. Such a small ϵ will be used to generate the reference data for all the examples discussed below. As shown in Figure 2, the old regularization scheme with a typical parameter $\epsilon = 10^{-8}$ gives a completely erroneous result.

As in our previous work, we measure the convergence of the result using a relative cumulative deviation (hereafter simply referred to as "deviation"), defined as

$$\text{deviation} = \frac{1}{P_{max} - P_{min}} \frac{1}{\tau} \int_0^\tau |P(t) - P_{ref}(t)|\, dt \tag{4.8}$$

where τ is the time scale of the simulation, $P_{ref}(t)$ is the reference result obtained by using $\epsilon = 10^{-32}$ in the new regularization scheme, P_{max} and P_{min} are the maximum and minimum values of $P_{ref}(t)$. The error tolerance of the predictor-corrector ODE solver was set such that there is $\sim 10^{-5}$ roundoff error in the deviation. Any deviation in this range can be considered as allowable numerical noise. For the numerical convergence of $P(t)$, we set the criterion that deviation be less than $\sim 10^{-4}$, which is stringent enough as compared with other convergence parameters and is still larger than the roundoff error. Finally, we measure the computational cost by the number of calls to the ML-MCTDH derivative subroutine.

Table 1 shows the performance for both the old and new regularization schemes. There are several clear messages. First, the typical regularization parameter $\epsilon = 10^{-8}$ does not work for either scheme. It simply cannot provide the quick rotation needed to adjust the initially unoccupied SPFs. As a result, not only is the accuracy terrible but also the cost is expensive. As ϵ decreases, both schemes provide better accuracy with actually reduced computational expense. However, even $\epsilon = 10^{-16}$ does not provide sufficient accuracy. This is bad news for the old regularization scheme, since such an ϵ is already near the double precision limit for this scheme. The first acceptable result is obtained with $\epsilon = 10^{-18}$ where both schemes give accurate enough results. However, the old scheme costs 2 orders of magnitude more and is obviously not practical. The new scheme, on the other hand, shows clear convergence with reasonable cost. For reference, the simulation that employs the new

Table 1. Number of Calls to the ML-MCTDH Derivative Subroutine and Deviation versus the Regularization Parameter ϵ[a]

	old regularization		new regularization	
ϵ	no. of calls	deviation	no. of calls	deviation
10^{-8}	165912	5.1×10^{-1}	161408	5.1×10^{-1}
10^{-10}	133369	5.0×10^{-1}	22317	3.7×10^{-1}
10^{-12}	21742	4.3×10^{-2}	16128	4.3×10^{-2}
10^{-14}	14321	2.7×10^{-2}	13895	7.9×10^{-3}
10^{-16}	97996	2.8×10^{-3}	12669	1.0×10^{-3}
10^{-18}	1536865	2.9×10^{-4}	14336	1.2×10^{-4}
10^{-20}			13834	4.8×10^{-5}
10^{-22}			19749	2.1×10^{-5}
10^{-24}			32387	1.4×10^{-5}
10^{-26}			39732	2.3×10^{-5}
10^{-28}			56707	7.4×10^{-6}
10^{-30}			76131	2.3×10^{-6}
10^{-32}			103485	reference

[a]The physical parameters are $\alpha = 2$, $D/\Delta = 0$, $\omega_c/\Delta = 25$. A seven-layer ML-MCTDH is used to treat a bath of 10 000 modes.

https://dx.doi.org/10.1021/acs.jpca.0c11221
J. Phys. Chem. A XXXX, XXX, XXX−XXX

regularization scheme with $\epsilon = 10^{-18}$ takes less than 3 h on a modest Intel core-i5 computer.

The above finding reveals a tough reality that for a large system the old regularization scheme may no longer be useful. This is confirmed from our investigations on a series of models with a different number of modes N. For this example the old regularization scheme works fine when $N < 500$, difficult but manageable in the range $1000 < N < 2000$ (with a small enough regularization parameter such as $\epsilon = 10^{-14}$), and becomes prohibitively expensive for larger N. It is essentially impractical to use the old scheme for $N > 5000$. Since most systems in previous applications of ML-MCTDH were well below this size, the defect of the old regularization scheme was not considered serious.

To illustrate the importance of employing the new regularization scheme on large systems, we show the results for the same physical parameters but obtained for a bath of 100 000 modes. Previously we tried to avoid a very deep layering, because such a calculation was difficult to converge. With the new regularization scheme, however, the use of a deeply layered ML-tree is no longer problematic and here we use the large number of 17 layers (18 layers if one considers MCTDH as a two layer approach). For simplicity we use a binary branching of the ML tree: the first layer contains two nodes, one for the bath and the other for the system states. The bath node is recursively bifurcated to the next 16 layers, thus generating 2^{15}–2^{16} bottom layer nodes (some branches are trimmed during the automatic layer construction.) Mode combination and basis contraction are again used for each bottom node, which contains at most 3 bath modes. The number of primitive basis functions range from 3 for high-frequency modes and 14 for low-frequency modes. We use the notation $(16 \times 8|4 \times 9)$ to denote the configuration setting such that there are 16 SPFs per node of each layer for the first 8 layers, and 4 SPFs per node of each layer for the next 9 layers. This is more than enough to reach convergence as for another much smaller setting $(6 \times 8|3 \times 9)$, the deviation is $\sim 10^{-4}$ from it.

Table 2 shows that numerically converged results can only be obtained when $\epsilon < 10^{-20}$ (which rules out the use of the old scheme). With a rather broad range $\epsilon \in [10^{-28}$ to $10^{-20}]$, the computational cost stays roughly the same and only doubles for the smallest $\epsilon = 10^{-32}$. This suggests the robustness of the new regularization scheme and its practicality for ML-MCTDH simulation of large systems. The calculations do become more expensive. With $\epsilon = 10^{-24}$, the $(16 \times 8|4 \times 9)$ configuration setting takes 85 h whereas the $(6 \times 8|3 \times 9)$ configuration setting takes 5 h on the same Intel core-i5 computer. Nevertheless, these calculations are manageable by modern standards.

One may notice that in Table 2 a smaller tolerance was set for the ODE integrator: 10^{-12} absolute and 10^{-8} relative. This is one of the reasons that calculations take more time steps in Table 2. It may be thought that a larger tolerance such as in Table 1 can be used to accelerate the calculations. Table 3 shows that it is not capable of providing accurate enough results. It is often tempting to cut corners by increasing the error tolerance of an integrator, but robustness and accuracy are more important in our point of view, especially when one uses ML-MCTDH to generate benchmark results.

Table 2. Number of Calls to the ML-MCTDH Derivative Subroutine and Deviation versus the Regularization Parameter ϵ[a]

ϵ	no. of calls	deviation
10^{-12}	231978	4.8×10^{-1}
10^{-14}	62546	5.4×10^{-2}
10^{-16}	50460	2.7×10^{-2}
10^{-18}	70927	3.7×10^{-3}
10^{-20}	135616	4.0×10^{-4}
10^{-22}	117491	2.9×10^{-5}
10^{-24}	126699	8.7×10^{-6}
10^{-26}	90164	5.2×10^{-5}
10^{-28}	119135	6.3×10^{-5}
10^{-30}	216717	1.3×10^{-6}
10^{-32}	256434	reference

[a]The physical parameters are $\alpha = 2$, $D/\Delta = 0$, $\omega_c/\Delta = 25$. A 17-layer ML-MCTDH is used to treat a bath of 100 000 modes. The configuration setting is $(16 \times 8|4 \times 9)$. For the ODE integrator the absolute tolerance is set to 10^{-12} and the relative tolerance is set to 10^{-8}. Only the results under the new regularization scheme are shown since the old scheme completely fails.

Table 3. Number of Calls to the ML-MCTDH Derivative Subroutine and Deviation versus the Regularization Parameter ϵ[a]

ϵ	no. of calls	deviation
10^{-12}	688706	5.3×10^{-1}
10^{-16}	237369	3.4×10^{-1}
10^{-20}	233597	3.4×10^{-1}
10^{-24}	45510	6.9×10^{-2}
10^{-28}	38658	1.2×10^{-2}
10^{-32}	37887	1.3×10^{-3}
10^{-34}	42490	4.8×10^{-4}

[a]A 17-layer ML-MCTDH is used to treat a bath of 100 000 modes. The parameters are the same as in Table 2 except for the ODE integrator the absolute tolerance is set to 10^{-10} and relative tolerance set to 10^{-6}. The reference result is the same as in Table 2.

The above results are obtained with a narrow but tall tree. One may think that because of this particular tree structure the old regularization scheme fails and the new regularization scheme requires a small $\epsilon < 10^{-20}$ to achieve convergence. To check this, we have exploited different tree structures and obtained almost the same finding. For example, for a wider tree where the first layer has 5 nodes and each subsequent layer contains at most 3 nodes, an 11-layer ML tree can accommodate 100 000 modes. Convergence is again only achieved when $\epsilon < 10^{-20}$. Thus, it is the number of degrees of freedom rather than the tree structure that demands a small regularization parameter.

IV.B. What about Weaker Couplings? The previous example of the spin−boson model is in a very strong coupling regime. A natural question is whether the integration is easier for a weaker coupling. Table 4 illustrates this for $\alpha = 0.5$, which is usually considered an intermediate coupling strength. Integration requires almost the same regularization parameter: $\epsilon < 10^{-18}$. The finding is similar from Table 5, which shows the result for $\alpha = 0.02$, a very weak coupling case. Convergence still requires $\epsilon < 10^{-18}$. All this suggests that with this many degrees of freedom, the old regularization scheme is no longer applicable. One has to employ the new regularization scheme with a small enough regularization parameter to obtain meaningful results.

https://dx.doi.org/10.1021/acs.jpca.0c11221
J. Phys. Chem. A XXXX, XXX, XXX−XXX

Table 4. Number of Calls to the ML-MCTDH Derivative Subroutine and Deviation versus the Regularization Parameter ϵ[a]

ϵ	no. of calls	deviation
10^{-12}	107117	2.8×10^{-1}
10^{-16}	27556	4.7×10^{-3}
10^{-18}	30696	1.0×10^{-4}
10^{-20}	33236	2.9×10^{-5}
10^{-24}	39708	5.4×10^{-5}
10^{-28}	54501	6.5×10^{-5}
10^{-32}	56211	reference

[a]A 17-layer ML-MCTDH is used to treat a bath of 100 000 modes. The configuration setting is $(8 \times 8|4 \times 9)$. The parameters are the same as in Table 2 except the coupling is weaker, $\alpha = 0.5$.

Table 5. Number of Calls to the ML-MCTDH Derivative Subroutine and Deviation versus the Regularization Parameter ϵ[a]

ϵ	no. of calls	deviation
10^{-12}	741946	1.2×10^{-2}
10^{-16}	96017	1.0×10^{-2}
10^{-18}	31791	5.1×10^{-4}
10^{-20}	38324	2.8×10^{-6}
10^{-24}	40767	6.6×10^{-7}
10^{-28}	46341	5.2×10^{-7}
10^{-32}	53031	reference

[a]A 17-layer ML-MCTDH is used to treat a bath of 100 000 modes. The configuration setting is $(8 \times 8|4 \times 9)$. The parameters are the same as in Table 2 except the coupling is weaker, $\alpha = 0.02$.

V. CONCLUSIONS

In this Perspective we have reviewed our recently proposed new scheme for regularizing the equations of motion for MCTDH and ML-MCTDH. Different from regularizing the reduced density matrix in the old scheme, the new approach regularizes the matrix unfolding of the coefficient tensor via the use of singular value decomposition. This allows a much faster adjustment of the virtual orbitals and allows them to be populated quickly. The new regularization scheme is much more important for ML-MCTDH simulations, because the SPFs of the upper layers of an ML-tree are of rather high dimensionality. This makes it likely that initially the virtual SPFs are orthogonal to their optimal form.[72−74] As long as they are orthogonal to what they should be, they cannot gain occupation. Only the new regularization scheme is able to rotate a truly unoccupied SPF into its optimal direction in Hilbert space (see Figure 1).

As the size of the simulation system becomes larger, the underlying whole Hilbert space becomes much larger than the subspace that ML-MCTDH simulation resides. This sparsity was coined as the "curse of dimensionality" by Bellman. As a result, variation calculations require a very fast exploitation of the correct Hilbert subspace. Our examples of the spin−boson model show that it becomes common to employ a very small regularization parameter to achieve numerical convergence. This has more to do with the size of the system than the coupling strength when the system is particularly large. While the spin−boson model has a simple Hamiltonian, it is similar (from the perspective of ML-MCTDH simulations) to vibronic coupling models used in many other applications such as computation of photoexcitation spectra,[7,78] photoionization spectra,[57,79] excitation energy transfer,[60] singlet fission,[61,62] and quantum transport.[34,35,49] The examples illustrated in this paper suggest that as the ML-MCTDH algorithm becomes mature enough to tackle bigger systems, it is time to adopt the new regularization scheme for its equations of motion.

ML-MCTDH employs a very general ansatz for the wave function, it is closely related to several other tensor network approaches. The manipulation of tree structures is in principle straightforward. For example, one may adopt a balanced tree in the first few layers and then use the tensor train format for deeper layers, or one can do it reversely.[80] These approaches are being explored by different researchers in different fields. We have experimented with several different tree structures and all of them require a careful use of the new regularization scheme. We thus believe that this is a rather general requirement for time-dependent tensor network applications to large systems. Of course, it is not easy to use a skewed tree such as the tensor train format to handle 100 000 modes, at least not for the moment. So the problem of correctly regularizing the equations of motion may not seem so urgent for some applications. However, our study shows that it is time to seriously consider this for realistic applications of ML-MCTDH.

AUTHOR INFORMATION

Corresponding Authors

Haobin Wang − *Department of Chemistry, University of Colorado Denver, Denver, Colorado 80217-3364, United States;* orcid.org/0000-0002-3532-7770; Email: haobin.wang@ucdenver.edu

Hans-Dieter Meyer − *Physikalisch-Chemisches Institut, Universität Heidelberg, D-69120 Heidelberg, Germany*; Email: Hans-Dieter.Meyer@pci.uni-heidelberg.de

Complete contact information is available at: https://pubs.acs.org/10.1021/acs.jpca.0c11221

Notes

The authors declare no competing financial interest.

Biographies

Haobin Wang obtained his BSc. from University of Science and Technology of China in 1991, majoring in Chemical Physics. He received his Ph.D. degree in Physical Chemistry from Wayne State University in 1996 and then did his postdoctoral research at University of California—Berkeley. He was an Assistant Professor of Chemistry at New Mexico State University from 2001 to 2006 and had been Professor there since 2011. In 2014, he joined the Chemistry Department of University of Colorado Denver. Dr. Wang's research has focused on developing computational methods to simulate quantum dynamics for large many-body systems.

Hans-Dieter Meyer did his undergraduate and graduate studies at the University Göttingen, Germany. He received his Ph.D. in 1978 while working with Prof. J. P. Toennies at the Max-Plank Institut für Strömungsforschung. He then carried out postdoctoral work with Professor William H. Miller at the University of California, Berkeley. In 1979 he went back to Göttingen and then, in 1980, further on to Heidelberg, where we worked as a scientific researcher. He habilitated 1991 in Heidelberg and became an apl Professor at the University Heidelberg in 2005. Prof. Meyer has worked on semiclassical methods, quantum chaos, electron−molecule scattering, and complex absorbing potentials (CAP). But over the last almost 30 years his research was more and more focused on the application and further development of the Multiconfiguration Time-Dependent Hartree (MCTDH) method.

https://dx.doi.org/10.1021/acs.jpca.0c11221
J. Phys. Chem. A XXXX, XXX, XXX−XXX

■ ACKNOWLEDGMENTS

H.W. acknowledges the support from the National Science Foundation CHE-1954639. This work used the Extreme Science and Engineering Discovery Environment (XSEDE), which is supported by NSF grant number ACI-1548562, and resources of the National Energy Research Scientific Computing Center (NERSC), which is supported by the Office of Science of the U.S. Department of Energy under Contract No. DE-AC02-05CH11231.

■ REFERENCES

(1) Manthe, U.; Meyer, H.-D.; Cederbaum, L. S. Wave-Packet Dynamics within the Multiconfiguration Hartree Framework: General Aspects and application to NOCl. *J. Chem. Phys.* **1992**, *97*, 3199−3213.
(2) Beck, M. H.; Jäckle, A.; Worth, G. A.; Meyer, H.-D. The multi-configuration time-dependent Hartree (MCTDH) method: A highly efficient algorithm for propagating wave packets. *Phys. Rep.* **2000**, *324*, 1−105.
(3) Meyer, H.-D.; Worth, G. A. Quantum molecular dynamics: Propagating wavepackets and density operators using the multi-configuration time-dependent Hartree (MCTDH) method. *Theor. Chem. Acc.* **2003**, *109*, 251−267.
(4) Meyer, H.-D., Gatti, F., Worth, G. A., Eds. *Multidimensional Quantum Dynamics: MCTDH Theory and Applications*; Wiley-VCH: Weinheim, 2009.
(5) Meyer, H.-D. Studying molecular quantum dynamics with the multiconfiguration time-dependent Hartree method. *WIREs: Comput. Mol. Sci.* **2012**, *2*, 351−374.
(6) Meyer, H.-D.; Manthe, U.; Cederbaum, L. S. The Multi-Configurational Time-Dependent Hartree Approach. *Chem. Phys. Lett.* **1990**, *165*, 73−78.
(7) Raab, A.; Worth, G.; Meyer, H.-D.; Cederbaum, L. S. Molecular dynamics of pyrazine after excitation to the S_2 electronic state using a realistic 24-mode model Hamiltonian. *J. Chem. Phys.* **1999**, *110*, 936−946.
(8) Wang, H. Basis set approach to the quantum dissipative dynamics: Application of the multiconfiguration time-dependent Hartree method to the spin-boson problem. *J. Chem. Phys.* **2000**, *113*, 9948−9956.
(9) Wang, H.; Thoss, M.; Miller, W. H. Systematic convergence in the dynamical hybrid approach for complex systems: A numerically exact methodology. *J. Chem. Phys.* **2001**, *115*, 2979−2990.
(10) Thoss, M.; Wang, H. Quantum dynamical simulation of ultrafast photoinduced electron transfer processes in a mixed-valence compound. *Chem. Phys. Lett.* **2002**, *358*, 298−306.
(11) Wang, H.; Thoss, M. Theoretical Study of Ultrafast Photoinduced Electron Transfer Processes in Mixed-Valence Systems. *J. Phys. Chem. A* **2003**, *107*, 2126−2136.
(12) Vendrell, O.; Gatti, F.; Lauvergnat, D.; Meyer, H.-D. Full dimensional (15D) quantum-dynamical simulation of the protonated water dimer I: Hamiltonian setup and analysis of the ground vibrational state. *J. Chem. Phys.* **2007**, *127*, 184302.
(13) Vendrell, O.; Gatti, F.; Meyer, H.-D. Full dimensional (15D) quantum-dynamical simulation of the protonated water dimer II: Infrared spectrum and vibrational dynamics. *J. Chem. Phys.* **2007**, *127*, 184303.
(14) Vendrell, O.; Brill, M.; Gatti, F.; Lauvergnat, D.; Meyer, H.-D. Full dimensional (15D) quantum-dynamical simulation of the protonated water dimer III: mixed Jacobi-valence parametrization and benchmark results for the zero-point energy, vibrationally excited states and infrared spectrum. *J. Chem. Phys.* **2009**, *130*, 234305.
(15) Vendrell, O.; Gatti, F.; Meyer, H.-D. Full dimensional (15D) quantum-dynamical simulation of the protonated water dimer IV: Isotope effects in the infrared spectra of $D(D_2O)_2^+$, $H(D_2O)_2^+$ and $D(H_2O)_2^+$ isotopologues. *J. Chem. Phys.* **2009**, *131*, 034308.
(16) Schröder, M.; Gatti, F.; Meyer, H.-D. Theoretical studies of the tunneling splitting of malonaldehyde using the multiconfiguration time-dependent Hartree approach. *J. Chem. Phys.* **2011**, *134*, 234307.
(17) Schröder, M.; Meyer, H.-D. Calculation of the vibrational excited states of malonaldehyde and their tunneling splittings with the multi-configuration time-dependent Hartree method. *J. Chem. Phys.* **2014**, *141*, 034116.
(18) Hammer, T.; Manthe, U. Intramolecular proton transfer in malonaldehyde: Accurate multilayer multi-configurational time-dependent Hartree calculations. *J. Chem. Phys.* **2011**, *134*, 224305.
(19) Hammer, T.; Manthe, U. Iterative diagonalization in the state-averaged multi-configurational time-dependent Hartree approach: Excited state tunneling splitting in malonaldehyde. *J. Chem. Phys.* **2012**, *136*, 054105.
(20) Schiffel, G.; Manthe, U. Quantum dynamics of the $H + CH_4 \rightarrow H_2 + CH_3$ reaction in curvilinear coordinates: Full-dimensional and reduced dimensional calculations of reaction rates. *J. Chem. Phys.* **2010**, *132*, 084103.
(21) Schiffel, G.; Manthe, U. Communications: A rigorous transition state based approach to state-specific reaction dynamics: Full-dimensional calculations for $H + CH_4 \rightarrow H_2 + CH_3$. *J. Chem. Phys.* **2010**, *132*, 191101.
(22) Schiffel, G.; Manthe, U. A transition state view on reactive scattering: Initial state-selected reaction probabilities for the $H + CH_4 \rightarrow H_2 + CH_3$ reaction studied in full dimensionality. *J. Chem. Phys.* **2010**, *133*, 174124.
(23) Welsch, R.; Manthe, U. Reaction dynamics with the multi-layer multi-configurational time-dependent Hartree approach: $H + CH_4 \rightarrow H_2 + CH_3$ rate constants for different potentials. *J. Chem. Phys.* **2012**, *137*, 244106.
(24) Welsch, R.; Manthe, U. The role of the transition state in polyatomic reactions: Initial state-selected reaction probabilities of the $H+CH_4 \rightarrow H_2+CH_3$ reaction. *J. Chem. Phys.* **2014**, *141*, 174313.
(25) Wang, H.; Thoss, M. Multilayer formulation of the multi-configuration time-dependent Hartree theory. *J. Chem. Phys.* **2003**, *119*, 1289−1299.
(26) Manthe, U. A multilayer multiconfigurational time-dependent Hartree approach for quantum dynamics on general potential energy surfaces. *J. Chem. Phys.* **2008**, *128*, 164116.
(27) Vendrell, O.; Meyer, H.-D. Multilayer multiconfiguration time-dependent Hartree method: Implementation and applications to a Henon-Heiles Hamiltonian and to pyrazine. *J. Chem. Phys.* **2011**, *134*, 044135.
(28) Wang, H. Multilayer Multiconfiguration Time-Dependent Hartree Theory. *J. Phys. Chem. A* **2015**, *119*, 7951−7965.
(29) Frenkel, J. *Wave Mechanics;;* Clarendon Press: Oxford, 1934.
(30) Wang, H.; Thoss, M. Numerically exact quantum dynamics for indistinguishable particles: The multilayer multiconfiguration time-dependent Hartree theory in second quantization representation. *J. Chem. Phys.* **2009**, *131*, 024114.
(31) Wang, H. Iterative Calculation of Energy Eigenstates Employing the Multilayer Multiconfiguration Time-Dependent Hartree Theory. *J. Phys. Chem. A* **2014**, *118*, 9253−9261.
(32) Wang, H.; Shao, J. Quantum Phase Transition in the Spin-Boson Model: A Multilayer Multiconfiguration Time-Dependent Hartree Study. *J. Phys. Chem. A* **2019**, *123*, 1882−1893.
(33) Wang, H.; Liu, X.; Liu, J. Accurate calculation of equilibrium reduced density matrix for the system-bath model: a multilayer multiconfiguration time-dependent Hartree approach and its comparison to a multi-electronic-state path integral molecular dynamics approach. *Chin. J. Chem. Phys.* **2018**, *31*, 446−456.
(34) Mendive-Tapia, D.; Mangaud, E.; Firmino, T.; de la Lande, A.; Desouter-Lecomte, M.; Meyer, H.-D.; Gatti, F. Multidimensional Quantum Mechanical Modeling of Electron Transfer and Electronic Coherence in Plant Cryptochromes: The Role of Initial Bath Conditions. *J. Phys. Chem. B* **2018**, *122*, 126−136.
(35) Wang, H.; Skinner, D. E.; Thoss, M. Calculation of reactive flux correlation functions for systems in a condensed phase environment: A multilayer multi-configuration time-dependent Hartree approach. *J. Chem. Phys.* **2006**, *125*, 174502.

https://dx.doi.org/10.1021/acs.jpca.0c11221
J. Phys. Chem. A XXXX, XXX, XXX−XXX

(36) Wang, H.; Thoss, M. Quantum dynamical simulation of electron-transfer reactions in an anharmonic environment. *J. Phys. Chem. A* **2007**, *111*, 10369−10375.
(37) Wang, H.; Thoss, M. Nonperturbative quantum simulation of time-resolved nonlinear spectra: Methodology and application to electron transfer reactions in the condensed phase. *Chem. Phys.* **2008**, *347*, 139−151.
(38) Wang, H.; Thoss, M. From coherent motion to localization: Dynamics of the spin-boson model at zero temperature. *New J. Phys.* **2008**, *10*, 115005.
(39) Song, X. G.; Wang, H.; Voorhis, T. V. A Langevin equation approach to electron transfer reactions in the diabatic basis. *J. Chem. Phys.* **2008**, *129*, 144502.
(40) Velizhanin, K. A.; Wang, H. Dynamics of electron transfer reactions in the presence of mode-mixing: Comparison of a generalized master equation approach with the numerically exact simulation. *J. Chem. Phys.* **2009**, *131*, 094109.
(41) Wang, H.; Thoss, M. From coherent motion to localization. II. Dynamics of the spin-boson model with sub-Ohmic spectral density at zero temperature. *Chem. Phys.* **2010**, *370*, 78−86.
(42) Zhou, Y.; Shao, J.; Wang, H. Dynamics of electron transfer in complex glassy environment modeled by the Cole-Davidson spectral density. *Mol. Phys.* **2012**, *110*, 581−594.
(43) Wang, H.; Shao, S. Dynamics of a two-level system coupled to a bath of spins. *J. Chem. Phys.* **2012**, *137*, 22A504.
(44) Tang, Z.; Ouyang, X.; Gong, Z.; Wang, H.; Wu, J. Extended hierarchy equation of motion for the spin-boson model. *J. Chem. Phys.* **2015**, *143*, 224112.
(45) Wang, H.; Thoss, M. A multilayer multiconfiguration time-dependent Hartree simulation of the reaction coordinate spin-boson model employing an interaction picture. *J. Chem. Phys.* **2017**, *146*, 124112.
(46) Yang, C.-H.; Denne, J.; Reed, S.; Wang, H. Computational study on the removal of photolabile protecting groups by photochemical reactions. *Comput. Theor. Chem.* **2019**, *1151*, 1−11.
(47) Velizhanin, K. A.; Wang, H.; Thoss, M. Heat transport through model molecular junctions: A multilayer multiconfiguration time-dependent Hartree approach. *Chem. Phys. Lett.* **2008**, *460*, 325−330.
(48) Wang, H.; Pshenichnyuk, I.; Härtle, R.; Thoss, M. Numerically exact, time-dependent treatment of vibrationally coupled electron transport in single-molecule junctions. *J. Chem. Phys.* **2011**, *135*, 244506.
(49) Wang, H.; Thoss, M. Numerically exact, time-dependent study of correlated electron transport in model molecular junctions. *J. Chem. Phys.* **2013**, *138*, 134704.
(50) Wang, H.; Thoss, M. Multilayer multiconfiguration time-dependent Hartree study of vibrationally coupled electron transport using the scattering-state representation. *J. Phys. Chem. A* **2013**, *117*, 7431−7441.
(51) Wang, H.; Thoss, M. On the Accuracy of the Noninteracting Electron Approximation for Vibrationally Coupled Electron Transport. *Chem. Phys.* **2016**, *481*, 117−123.
(52) Wang, H.; Thoss, M. Employing an interaction picture to remove artificial correlations in multilayer multiconfiguration time-dependent Hartree simulations. *J. Chem. Phys.* **2016**, *145*, 164105.
(53) Wang, H.; Thoss, M. A multilayer multiconfiguration time-dependent Hartree study of the nonequilibrium Anderson impurity model at zero temperature. *Chem. Phys.* **2018**, *509*, 13−19.
(54) Yang, C.-H.; Wang, H. Heat Transport in a Spin-Boson Model at Low Temperatures: A Multilayer Multiconfiguration Time-Dependent Hartree Study. *Entropy* **2020**, *22*, 1099.
(55) Meng, Q.; Meyer, H.-D. Lattice effects of surface cell: Multilayer multiconfiguration time-dependent Hartree study on surface scattering of CO/Cu(100). *J. Chem. Phys.* **2017**, *146*, 184305.
(56) Westermann, T.; Brodbeck, R.; Rozhenko, A. B.; Schoeller, W.; Manthe, U. Photodissociation of methyl iodide embedded in a host-guest complex: A full dimensional (189D) quantum dynamics study of CH_3I@resorc[4]arene. *J. Chem. Phys.* **2011**, *135*, 184102.
(57) Meng, Q.; Meyer, H.-D. A multilayer MCTDH study on the full dimensional vibronic dynamics of naphthalene and anthracene cations. *J. Chem. Phys.* **2013**, *138*, 014313.
(58) Schulze, J.; Kühn, O. Explicit correlated exciton-vibrational dynamics of the FMO complex. *J. Phys. Chem. B* **2015**, *119*, 6211−6216.
(59) Schulze, J.; Shibl, M. F.; Al-Marri, M. J.; Kühn, O. Multi-Layer multi-configuration time-dependent Hartree (ML-MCTDH) approach to the correlated exciton-vibrational dynamics in the FMO complex. *J. Chem. Phys.* **2016**, *144*, 185101.
(60) Shibl, M. F.; Schulze, J.; Al-Marri, M. J.; Kühn, O. Multilayer-MCTDH approach to the energy transfer dynamics in the LH2 antenna complex. *J. Phys. B: At., Mol. Opt. Phys.* **2017**, *50*, 184001.
(61) Zheng, J.; Xie, Y.; Jiang, S.; Lan, Z. Ultrafast Nonadiabatic Dynamics of Singlet Fission: Quantum Dynamics with the Multilayer Multiconfigurational Time-Dependent Hartree (ML-MCTDH) Method. *J. Phys. Chem. C* **2016**, *120*, 1375−1389.
(62) Reddy, S. R.; Coto, P. B.; Thoss, M. Intramolecular Singlet Fission: Insights from Quantum Dynamical Simulations. *J. Phys. Chem. Lett.* **2018**, *9*, 5979−5986.
(63) Tucker, L. R. Some mathematical notes of three-mode factor analysis. *Psychometrika* **1966**, *31*, 279−311.
(64) Grasedyck, L. Hierarchical singular value decomposition of tensors. *SIAM. J. Matrix Anal. & Appl.* **2010**, *31*, 2029−2054.
(65) Grasedyck, L.; Kressner, D.; Tobler, C. A literature survey of low−rank tensor approximation techniques. *GAMM − Mitteilungen* **2013**, *36*, 53−78.
(66) Lubich, C.; Rohwedder, T.; Schneider, R.; Vandereycken, B. Dynamical Approximation by Hierarchical Tucker and Tensor-Train Tensors. *SIAM J. Matrix Anal. Appl.* **2013**, *34*, 470−494.
(67) Schollwöck, U. The density-matrix renormalization group in the age of matrix product states. *Ann. Phys.* **2011**, *326*, 96−192.
(68) Meyer, H. D.; Wang, H. On regularizing the MCTDH equations of motion. *J. Chem. Phys.* **2018**, *148*, 124105.
(69) Wang, H.; Meyer, H.-D. On regularizing the ML-MCTDH equations of motion. *J. Chem. Phys.* **2018**, *149*, 044119.
(70) Lubich, C. Time integration in the multiconfiguration time-dependent Hartree method of molecular quantum dynamics. *Appl. Math. Res. Express* **2015**, *2015*, 311−328.
(71) Kloss, B.; Burghardt, I.; Lubich, C. Implementation of a novel projector-splitting integrator for the multi-configurational time-dependent Hartree approach. *J. Chem. Phys.* **2017**, *146*, 174107.
(72) Manthe, U. The multi-configurational time-dependent Hartree approach revisited. *J. Chem. Phys.* **2015**, *142*, 244109.
(73) Lee, K.-S.; Fischer, U. R. Truncated many-body dynamics of interacting bosons: A varitional principle with error monitoring. *Int. J. Mod. Phys. B* **2014**, *28*, 1550021.
(74) Mendive-Tapia, D.; Meyer, H.-D. Regularizing the MCTDH equations of motion through an optimal choice on-the-fly (i.e. spawning) of unoccupied single-particle functions. *J. Chem. Phys.* **2020**, *153*, 234114.
(75) Unfortunately, there are two different ways of counting layers. The first one simply counts the nodes (circles in an ML-tree) from top to bottom. In this case, MCTDH is equivalent to a two-layer ML-MCTDH approach. The second way ignores the top node. The number of layers is thus reduced by one and MCTDH becomes equivalent to a one-layer ML-MCTDH approach. This second way of counting is assumed when discussing the spin-boson examples, section IV.
(76) Leggett, A. J.; Chakravarty, S.; Dorsey, A. T.; Fisher, M. P. A.; Garg, A.; Zwerger, W. Dynamics of the dissipative two-state System. *Rev. Mod. Phys.* **1987**, *59*, 1−85.
(77) Weiss, U. *Quantum Dissipative Systems*, third ed.; World Scientific Publishing: Singapore, 2008.
(78) Gromov, E. V.; Trofimov, A. B.; Vitkovskaya, N. M.; Köppel, H.; Schirmer, J.; Meyer, H.-D.; Cederbaum, L. S. Theoretical study of excitations in furan: Spectra and molecular dynamics. *J. Chem. Phys.* **2004**, *121*, 4585−4598.

https://dx.doi.org/10.1021/acs.jpca.0c11221
J. Phys. Chem. A XXXX, XXX, XXX−XXX

(79) Baldea, I.; Köppel, H. Multistate multimode vibronic dynamics: entanglement of electronic and vibrational degrees of freedom in the benzene radical cation. *J. Chem. Phys.* **2006**, *124*, 064101.
(80) Kurashige, Y. Matrix product state formulation of the multiconfiguration time-dependent Hartree theory. *J. Chem. Phys.* **2018**, *149*, 194114.

https://dx.doi.org/10.1021/acs.jpca.0c11221
J. Phys. Chem. A XXXX, XXX, XXX−XXX